Tough, Bio-Inspired Hybrid Materials
E. Munch, *et al.*
Science **322**, 1516 (2008);
DOI: 10.1126/science.1164865

the dynamics of specific proteins. Cells respond to the drug by highly specific translocation events that correspond to the drug mode of action. Observation of these effects was enabled by measuring the proteome dynamics in space and time in individual cells. The present approach provides a window into human cell biology and opens the way for understanding how seemingly identical cells show different responses to signals and drugs.

References and Notes

1. K. A. Janes *et al.*, *Science* **310**, 1646 (2005).
2. J. R. Newman *et al.*, *Nature* **441**, 840 (2006).
3. A. Belle, A. Tanay, L. Bitincka, R. Shamir, E. K. O'Shea, *Proc. Natl. Acad. Sci. U.S.A.* **103**, 13004 (2006).
4. W. K. Huh *et al.*, *Nature* **425**, 686 (2003).
5. Z. E. Perlman *et al.*, *Science* **306**, 1194 (2004).
6. P. Yeh, A. I. Tschumi, R. Kishony, *Nat. Genet.* **38**, 489 (2006).
7. D. W. Young *et al.*, *Nat. Chem. Biol.* **4**, 59 (2008).
8. Y. Pommier, *Nat. Rev. Cancer* **6**, 789 (2006).
9. J. W. Jarvik *et al.*, *Biotechniques* **33**, 852 (2002).
10. J. W. Jarvik, C. A. Telmer, *Annu. Rev. Genet.* **32**, 601 (1998).
11. J. W. Jarvik, S. A. Adler, C. A. Telmer, V. Subramaniam, A. J. Lopez, *Biotechniques* **20**, 896 (1996).
12. A. Sigal *et al.*, *Nature* **444**, 643 (2006).
13. A. Sigal *et al.*, *Nat. Methods* **3**, 525 (2006).
14. A. Sigal *et al.*, *Nat. Protocols* **2**, 1515 (2007).
15. Materials and methods are available as supporting material on *Science* Online.
16. U. S. Eggert, T. J. Mitchison, *Curr. Opin. Chem. Biol.* **10**, 232 (2006).
17. C. J. Echeverri, N. Perrimon, *Nat. Rev. Genet.* **7**, 373 (2006).
18. S. G. Megason, S. E. Fraser, *Cell* **130**, 784 (2007).
19. R. Pepperkok, J. Ellenberg, *Nat. Rev. Mol. Cell Biol.* **7**, 690 (2006).
20. L. Trinkle-Mulcahy, A. I. Lamond, *Science* **318**, 1402 (2007).
21. P. J. Clyne, J. S. Brotman, S. T. Sweeney, G. Davis, *Genetics* **165**, 1433 (2003).
22. X. Morin, R. Daneman, M. Zavortink, W. Chia, *Proc. Natl. Acad. Sci. U.S.A.* **98**, 15050 (2001).
23. S. D. Desai, L. F. Liu, D. Vazquez-Abad, P. D'Arpa, *J. Biol. Chem.* **272**, 24159 (1997).
24. M. T. Muller, W. P. Pfund, V. B. Mehta, D. K. Trask, *EMBO J.* **4**, 1237 (1985).
25. J. S. Andersen *et al.*, *Nature* **433**, 77 (2005).
26. K. Kalita, D. Makonchuk, C. Gomes, J. J. Zheng, M. Hetman, *J. Neurochem.* **105**, 2286 (2008).
27. R. Sakasai *et al.*, *Genes Cells* **11**, 237 (2006).
28. V. M. Vassin, M. S. Wold, J. A. Borowiec, *Mol. Cell. Biol.* **24**, 1930 (2004).
29. M. Kaern, T. C. Elston, W. J. Blake, J. J. Collins, *Nat. Rev. Genet.* **6**, 451 (2005).
30. M. B. Elowitz, A. J. Levine, E. D. Siggia, P. S. Swain, *Science* **297**, 1183 (2002).
31. E. M. Ozbudak, M. Thattai, I. Kurtser, A. D. Grossman, A. van Oudenaarden, *Nat. Genet.* **31**, 69 (2002).
32. A. Bar-Even *et al.*, *Nat. Genet.* **38**, 636 (2006).
33. E. R. Parrilla-Castellar, S. J. Arlander, L. Karnitz, *DNA Repair (Amsterdam)* **3**, 1009 (2004).
34. L. Yang, C. Lin, S. Y. Sun, S. Zhao, Z. R. Liu, *Oncogene* **26**, 6082 (2007).
35. E. S. Witze, W. M. Old, K. A. Resing, N. G. Ahn, *Nat. Methods* **4**, 798 (2007).
36. R. Aebersold, M. Mann, *Nature* **422**, 198 (2003).
37. S. Ghaemmaghami *et al.*, *Nature* **425**, 737 (2003).

38. We thank the Kahn Family Foundation and the Israel Science Foundation for support. We thank E. Zalckvar, J. Bar, I. Glinert, T. Shlapok, and members of the Alon laboratory for discussions. The work of M.F.-M. and E.E. is supported by the Yeshaya Horowitz Association through the Center for Complexity Science.

Supporting Online Material

www.sciencemag.org/cgi/content/full/1160165/DC1
Materials and Methods
SOM Text
Figs. S1 to S20
Tables S1 to S4
References
Movies S1 to S4

7 May 2008; accepted 31 October 2008
Published online 20 November 2008;
10.1126/science.1160165
Include this information when citing this paper.

Tough, Bio-Inspired Hybrid Materials

E. Munch,[1] M. E. Launey,[1] D. H. Alsem,[1,2] E. Saiz,[1] A. P. Tomsia,[1] R. O. Ritchie[1,3]*

The notion of mimicking natural structures in the synthesis of new structural materials has generated enormous interest but has yielded few practical advances. Natural composites achieve strength and toughness through complex hierarchical designs that are extremely difficult to replicate synthetically. We emulate nature's toughening mechanisms by combining two ordinary compounds, aluminum oxide and polymethyl methacrylate, into ice-templated structures whose toughness can be more than 300 times (in energy terms) that of their constituents. The final product is a bulk hybrid ceramic-based material whose high yield strength and fracture toughness [~200 megapascals (MPa) and ~30 MPa·m$^{1/2}$] represent specific properties comparable to those of aluminum alloys. These model materials can be used to identify the key microstructural features that should guide the synthesis of bio-inspired ceramic-based composites with unique strength and toughness.

The quest for more-efficient energy-related technologies necessitates the development of lightweight, high-performance structural materials with exceptional strength and toughness. Unfortunately, these two properties tend to be mutually exclusive, and attaining optimal mechanical performance is invariably a compromise often achieved through the empirical design of microstructures. Nature has long developed the ability to combine brittle minerals and organic molecules into hybrid composites with exceptional fracture resistance and structural capabilities (*1*–*3*); indeed, many natural materials like bone, wood, and nacre (abalone shell) have highly sophisticated structures with complex hierarchical designs whose properties far exceed what could be expected from a simple mixture of their components (*2*, *4*). Biological mineralized composites, in particular bone, dentin, and nacre (*5*–*7*), can generate fracture toughness (resistance to the initiation and growth of a crack) primarily by extrinsic toughening mechanisms (*8*) that "shield" any crack from the applied loads. These mechanisms—which are quite different from those that toughen metals, for example—are created over so many dimensions (nano to macro) that it makes them very difficult to replicate in a synthetic material. From a fracture mechanics perspective, the presence of these mechanisms results in characteristic crack resistance-curve (R curve) behavior such that the fracture resistance actually increases with crack extension; that is, these materials develop their toughening primarily during crack growth, not during crack initiation. A prime example is nacre, which consists of 95 vol. % of layered aragonite ($CaCO_3$) platelets bonded by a thin layer of organic material, yet exhibits a toughness (in energy terms) some three orders of magnitude higher than that of calcium carbonate (*2*). The hard aragonite provides strength, but without a means to dissipate strain, nacre would be brittle; however, large inelastic deformation generated by interlayer shearing through the organic phase allows for such strain redistribution (*9*), so that toughness is achieved through viscoplastic energy dissipation in the organic layer associated with the controlled, yet limited, sliding of the aragonite layers over each other. Although there is controversy over the mechanisms that restrain sliding—resistance from the lamellae nanoroughness (*10*), plastic deformation of the aragonite at the nanolevel (*11*), the organic layer acting as a viscoelastic glue (*12*), or from the presence of mineral bridges (*2*, *13*)—the resulting toughness is remarkable. Attempts have been made to simulate this in synthetic materials, such as lamellar materials fabricated with conventional processing (tape or slip casting); however, the resulting layer thicknesses are typically more than two orders of magnitude larger than the ~0.5-μm aragonite platelet spacing in nacre (*14*, *15*). Such submicrometer layer spacings can be achieved by physical or chemical deposition, but not for bulk materials, because the techniques are restricted to the fabrication of thin films (*16*–*19*).

Processing strategy. Here, we apply this natural concept of hierarchical design to ceramic/polymer [Al_2O_3/PMMA (polymethyl methacrylate)] hybrid materials, which we fabricate in bulk form by freeze casting (*20*–*24*). Using controlled freezing of ceramic-based suspensions in wa-

[1]Materials Sciences Division, Lawrence Berkeley National Laboratory, Berkeley, CA 94720, USA. [2]National Center for Electron Microscopy, Lawrence Berkeley National Laboratory, Berkeley, CA 94720, USA. [3]Department of Materials Science and Engineering, University of California, Berkeley, CA 94720, USA.

*To whom correspondence should be addressed. E-mail: roritchie@lbl.gov

ter, we form large porous ceramic scaffolds (fig. S1) with architectures that are templated by the ice crystals. We first use directional freezing to promote the formation of lamellar ice with prescribed dimensions; this acts as the "negative" for creation of the layered ceramic scaffolds, which are subsequently infiltrated with the polymeric second phase. In addition to making lamellar structures, we also fabricate nacre-like "brick-and-mortar" structures, with very high ceramic content, by subsequently pressing the scaffolds in the direction perpendicular to the lamellae in order to collapse them, followed by a second sintering step to promote densification and the formation of ceramic bridges between the "bricks" (fig. S2). Using such techniques, we have made complex hierarchical architectures that allow us to refine the lamellae thickness, control their macroscopic orientation, manipulate the chemistry and roughness of the inter-lamellae interfaces, and generate a given density of inorganic bridges, all over a range of size scales.

In an attempt to replicate the microstructural design of nacre, we reduced the average lamellae thickness to 5 μm (which is still ~10 times thicker than the natural material) and used sucrose as an additive to the ceramic slurries (Fig. 1, A and B). Sucrose modifies the viscosity and phase diagram of the solvent, resulting in the formation of ice crystals with a characteristic microscopic roughness and bridge density similar to that in nacre (Fig. 1, C and D). Control of the lamellae roughness provided a mechanical means to manipulate adhesion at the inorganic/organic layer interfaces. This can be complemented at the molecular level by chemically grafting a methacrylate group onto the ceramic surfaces before PMMA infiltration using in situ free-radical polymerization; the presence of the methacrylate groups then acts to promote stronger covalent bonding between the two phases (Fig. 2 and fig. S2). To achieve a macroscopic alignment of the lamellae similar to that in nacre (over millimeter

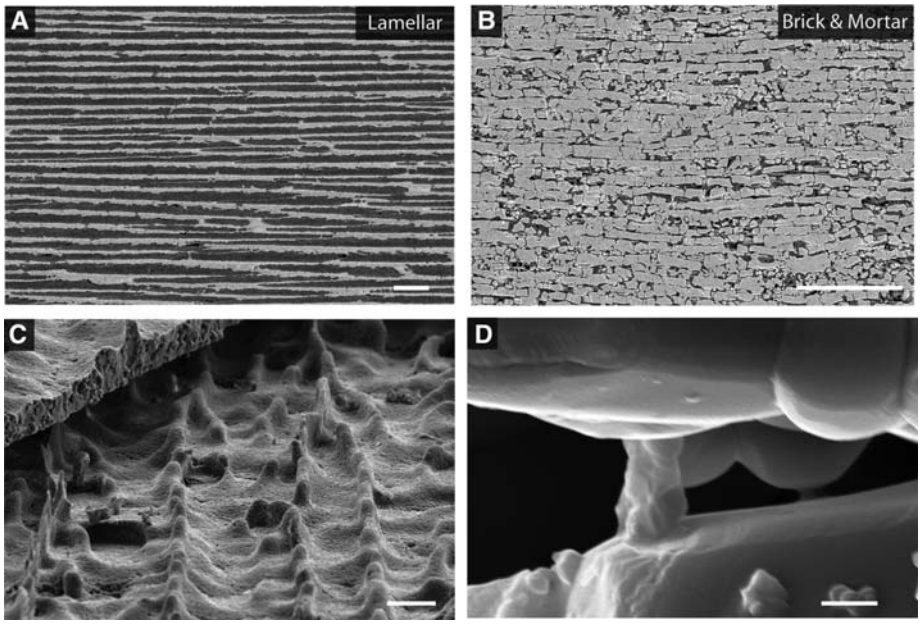

Fig. 1. Structure of ice-templated materials. (**A**) Al_2O_3/PMMA lamellar composites have been fabricated by freeze casting of ceramic suspensions followed by polymer infiltration (the lighter phase is the ceramic; the dark phase is the polymer). (**B**) Brick-and-mortar architectures are prepared through pressing of the lamellar materials and subsequent sintering and have much larger ceramic contents (up to 80 vol. %). (**C**) When sucrose is used as an additive to the freeze-casting slurry, the growing ice crystals develop a characteristic surface topography that translates into a microscopic roughness in the ceramic walls. (**D**) The process also results in the formation of ceramic bridges between lamellae (due to the trapping of ceramic particles by the growing ice) or bricks (the bridges form during the second sintering steps). By limiting sliding, they provide very effective toughening mechanisms in natural and synthetic materials. The alumina grain size inside the lamellae or bricks is ~1 μm. Scale bars: 100 μm [(A) and (B)], 10 μm (C), and 600 nm (D).

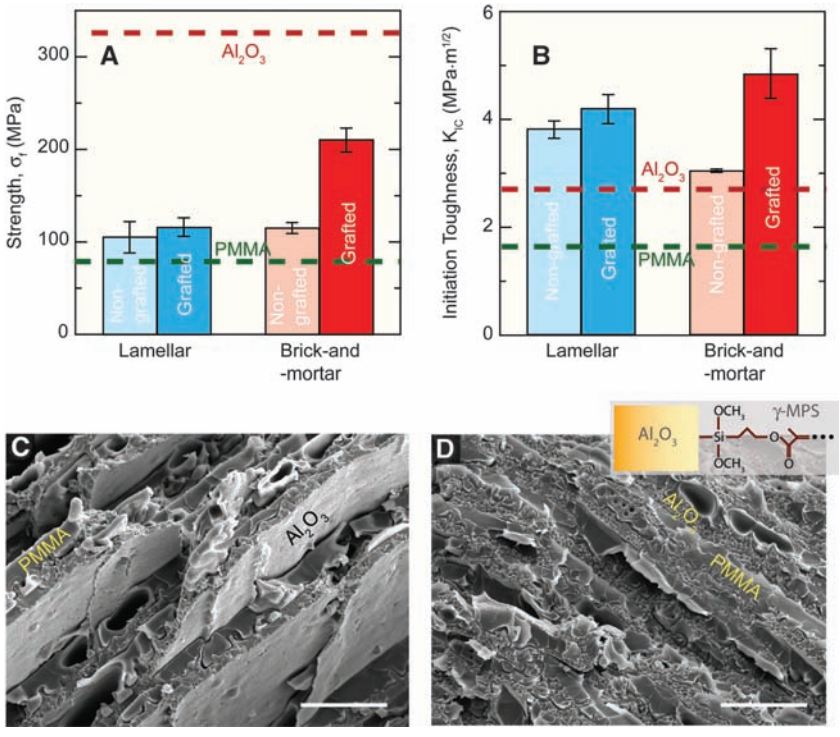

Fig. 2. Influence of interfacial chemistry on the mechanical response. (**A**) The strength of the hybrid composites can reach values above 200 MPa. (**B**) The crack-initiation fracture toughness, K_{IC}, can be up to twice that of the materials components. Chemical grafting increases the adhesion at the organic/inorganic interface and enhances both strength and initiation toughness. The error bars represent ±SD. (**C**) The scanning electron micrograph (SEM) of the fracture surface of a lamellar material with nongrafted interfaces (which leads to weaker boundaries) shows extensive interface delamination during fracture. (**D**) Chemical grafting (inset) results in better adhesion (stronger boundaries) and fracture surfaces that are much flatter. Scale bars indicate 5 μm [(C) and (D)].

dimensions or more), we patterned the cold finger on which the ice nucleates using parallel, ~40 μm, grooves. Brick-and-mortar architectures, prepared through pressing of the lamellar materials and subsequent sintering, have a much larger ceramic content (up to 80 vol. %). The ceramic "bricks" are 5 to 10 μm wide and 20 to 100 μm long. Although the polymer layers have an overall average thickness of ~1 to 2 μm, there are large areas in which the alumina bricks are separated by submicrometer polymer films similar to the microstructure of natural nacre (Fig. 3D). After infiltrating these porous scaffolds with the polymer, we produced a series of Al_2O_3/PMMA hybrid composites (Fig. 1, A and B), with hierarchical structures spanning multiple length scales that exhibit distinctive structural and mechanistic features similar to those in nacre.

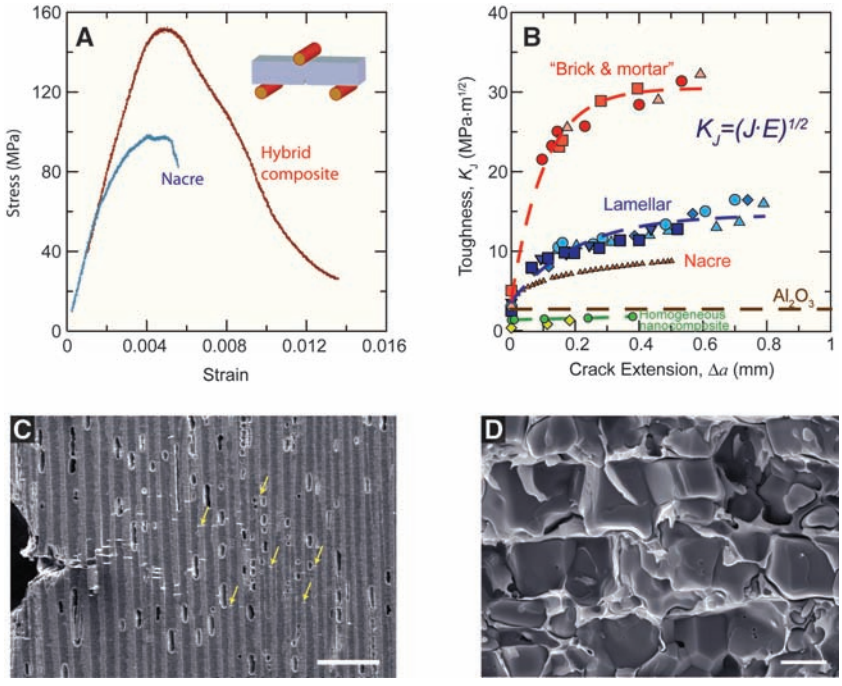

Fig. 3. Mechanical response and toughening mechanisms in the synthetic hybrid composites. (**A**) Bending stress-strain curves for the Al_2O_3/PMMA hybrid materials mimic those of nacre and show >1% inelastic deformation before failure. The curves correspond to nongrafted lamellar hybrid composite and hydrated nacre (abalone shell). (**B**) These materials show exceptional toughness for crack growth, similar to natural composites, and display significant rising R-curve behavior. Almost negligible toughening is observed in nanocomposites consisting of 500 nm Al_2O_3 particles dispersed in PMMA. (**C**) Scanning electron micrograph taken during an in situ R-curve measurement of a lamellar structure. The image taken during crack propagation shows two of the toughening mechanisms acting at large scales: the wide distribution of damage (over millimeter dimensions) in the form of contained microcracking within the ceramic layers (yellow arrows point to some of these microcracks) and the voids in the polymer layers. (**D**) Fracture surface of a grafted brick-and-mortar structure. Controlled sliding contributes to a rise of the crack-growth toughness to values that can be >300 times higher (in energy terms) than that of Al_2O_3. In addition to the roughness of the ceramic surfaces and the inorganic bridges between ceramic bricks, a principal reason for the controlled sliding is the presence of a submicrometer polymer film between alumina blocks. Scale bars: 250 μm (C) and 3 μm (D).

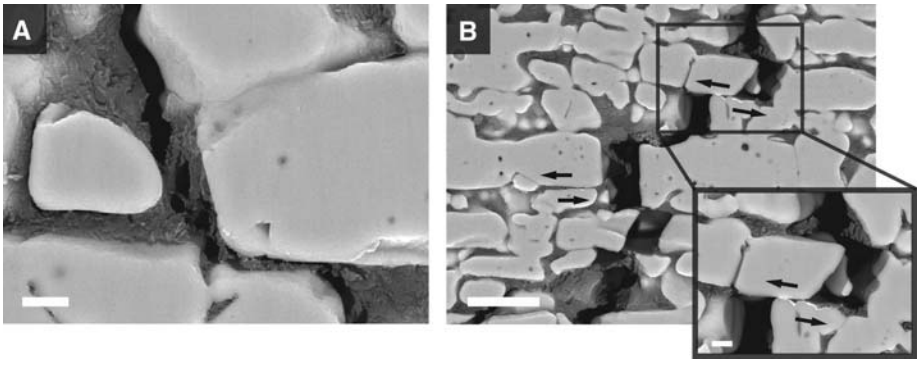

Fig. 4. Toughening mechanisms in brick-and-mortar microstructures. In situ imaging of crack propagation in brick-and-mortar structures shows clear evidence of (**A**) polymer tearing and stretching over micrometer dimensions (as have also been observed in the organic phase of nacre) and (**B**) "pull out" and frictional sliding between ceramic bricks (inset; arrows indicate the direction of sliding). The thin bright lines between the sliding grains in the inset indicate electrical charging in the SEM resulting from the deformation of the gold coating during sliding. Scale bars: 2 μm [(A) and the inset in (B)] and 10 μm (B).

Replicating the mechanical response of natural structures. Matching the structural features of natural materials is not easy, but attaining their unique combinations of mechanical properties is much more difficult and has rarely been achieved. In natural and biological materials, desired properties are often achieved in a directional fashion (*2*, *25*); indeed, certain engineering materials have also been optimized with highly anisotropic properties, as in multilayer ceramic armor materials to laminated epoxy/carbon fiber composites and directionally solidified turbine blade alloys for aerospace engineering (*26*–*28*). Similarly, the flexural strengths of our ice-templated hybrid materials are high in the direction perpendicular to the lamellae and comparable to that of alumina, with values of 120 to 210 MPa for the lamellae and brick-and-mortar structures, respectively (Fig. 2A). More importantly though, corresponding plane-strain K_{Ic} fracture toughnesses (which represent values for crack initiation) are almost double of what could be expected from the simple "rule of mixtures" of Al_2O_3 and PMMA (Fig. 2B). The reference alumina values here correspond to bulk samples prepared by slip casting in our laboratory. The suspensions for slip-casting and freeze casting use the same starting powders and similar solid contents with identical sintering cycles (*29*). Slip casting was selected because, as for freeze casting, the ceramic sample forms through the packing of powders from a liquid suspension.

Whereas grafting to improve Al_2O_3/PMMA interface adhesion (Fig. 2, C and D) resulted in a mildly higher strength and initiation toughness for lamellar structures, a very significant increase was seen for the brick-and-mortar structure (Fig. 2, A and B). However, the most notable feature of our synthetic composites is that they replicate the mechanical behavior of natural materials; specifically, they display large (>1%) inelastic strains when loaded in tension (Fig. 3A) and develop exceptional toughness for crack growth (Fig. 3B). Like many hard mineralized biocomposites, the ice-templated materials exhibit a high degree of inelasticity, despite the brittle nature of their main ceramic constituent. Although single-value linear-elastic parameters based on crack initiation, such as K_{Ic}, have traditionally been used to quantify toughness, they cannot capture, or even represent, the multiple length-scale toughening acting in these compos-

ites that lead to their characteristic R-curve behavior where the fracture resistance actually increases with crack extension. Human cortical bone, for example, derives more than 75% of its toughness during crack growth, which is not reflected in its reported K_{Ic} toughness value of 2 to 7 MPa·m$^{1/2}$; the true toughness of bone (in the transverse orientation) exceeds 20 MPa·m$^{1/2}$ when the crack-growth toughening contributions are taken into account (*25*). To evaluate the toughness of these materials requires nonlinear elastic fracture mechanics to characterize the contributions from inelastic deformation and, more importantly, R-curve analysis to characterize the toughness associated with crack growth, both of which are afforded by the use of the *J*-R curve. Our brick-and-mortar structures consist of ~80% alumina yet display a remarkable 1.4% strain to failure. Accordingly, we used the *J*-R curve approach to fully define their toughness properties. The results (plotted for comparison in terms of a stress intensity K_J back-calculated from the *J* measurements) are shown in Fig. 3B, where it is apparent that both natural (nacre) and our synthetic composites exhibit extensive rising R-curve behavior indicative of extensive extrinsic toughening. The degree of toughening in our hybrid composites clearly surpasses that of nacre (the often cited "gold standard" in biomimetic design). Our Al_2O_3/PMMA lamellar and brick-and-mortar structures reach (steady-state) fracture toughnesses K_{Jc} of 15 MPa·m$^{1/2}$ (J_c ~ 5000 J/m^2) and 30 MPa·m$^{1/2}$ (J_c ~ 8000 J/m^2), respectively. The latter value is an outstandingly high toughness for a material consisting of 80% alumina with a strength above 200 MPa; it far exceeds the toughness of either constituent. Indeed, the toughnesses of our best hybrid materials are an order of magnitude higher than standard homogeneous nanocomposites consisting of 500 nm Al_2O_3 particles dispersed in PMMA with the same nominal composition. Similar to the fine-grained (1 μm) alumina, these homogeneous Al_2O_3/PMMA composites display minimal extrinsic toughening and consequently no rising R-curve behavior, with characteristically very low fracture toughness, below 2 MPa·m$^{1/2}$ (Fig. 3B). We believe that this result illustrates the importance of hierarchical design in promoting toughening mechanisms at multiple length scales as a way to create materials with unique combinations of strength and fracture resistance.

Confluence of toughening mechanisms. Mechanistically, we can identify the salient sources of toughening in these hybrid composites by performing additional fracture toughness tests in situ in the scanning electron microscope. This technique allows us to quantitatively measure the R-curve while simultaneously monitoring the evolution of damage mechanisms ahead of the crack tip and extrinsic toughening mechanisms that result in the wake; furthermore, we can image in real time how these mechanisms are affected by the materials architecture (*25*). Our results show a confluence of toughening mechanisms acting at several length scales, as in biological materials. Similar to nacre, the microstructural damage is not localized but rather is widely distributed over very large (millimeter-scale) dimensions (Fig. 3C). In general, in addition to inelastic deformation within the polymer, which can be seen in the form of micrometer-scale tearing in Fig. 4A, this damage principally takes the form of multiple microcracks contained within the ceramic layers. There are also elongated voids within the polymeric interlayers, many of which result from the processing, but which appear to promote local plastic flow and grow during loading. These brittle and ductile damage processes appear to be distinct, with little evidence of interaction. The presence of such damage initiated ahead of (and distinct from) the main growing crack leads to the formation of so-called uncracked-ligament bridging (*30*) in the wake of the crack tip. These elastic bridges (which are distinct from the preexisting ceramic bridges between layers) are formed in situ before the main growing crack links to the microcracks and voids; the bridges effectively span the crack and carry load that would otherwise be used to promote macroscopic crack advance (*31*). Notably, this mechanism is one of the major origins of toughness in cortical bone and tooth dentin (*6*, *7*), as well as in rocks and metal-matrix composites (*30*). In addition, the elongated voids in the polymeric layers (Fig. 3C) can act as very effective local crack arresters, as with the well-known Cook-Gordon mechanism (*32*) in laminates; furthermore, the energy dissipation required to break the resulting crack bridges leads to ductile-phase toughening (*33*), which is a common source of fracture resistance in polymer- and metal-matrix composites. Accordingly, through control of the structural architecture at several length scales, we have combined a number of toughening mechanisms operating over a large range of dimensions to generate extensive crack-tip shielding and hence unprecedented fracture resistance for a ceramic-based material.

The difference in the lamellar versus the brick-and-mortar structures lies in the precise nature and relative contribution of these toughening mechanisms. In the lamellar composites, chemical grafting of the organic-inorganic interfaces does not appear to have too much of an effect. However, the weaker Al_2O_3/PMMA (nongrafted) interfaces are observed to promote crack deflection and "delamination" along the interface (Fig. 2, C and D). This facilitates the formation of uncracked-ligament bridging (as described above), as well as frictional sliding ("sliding interference") along the rough debonded interface, with consequent energy dissipation associated with deformation within the soft phase. The situation is different for the brick-and-mortar structures, for which the highest fracture toughness of >30 MPa·m$^{1/2}$ is achieved with high-strength, grafted interfaces. As with the lamellar materials, the brick-and-mortar microstructures exhibit extensive elastic bridging; however, unlike the lamellar materials, there is no fracture of the ceramic bricks; rather, there is some degree of "pull-out" between the bricks that in some respects replicates at microscopic dimensions the nanoscale phenomena observed in nacre (Fig. 4) (*34*). This form of toughening is particularly potent and the prime source of the fracture resistance

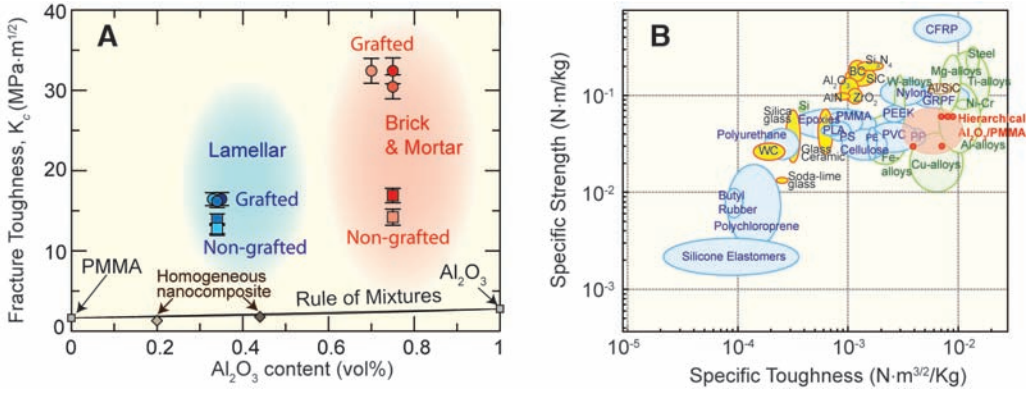

Fig. 5. Specific strength/toughness properties of hybrid composites comparable to aluminum alloys. (**A**) Fracture toughness for lamellar and brick-and-mortar composites. The toughness of the pure components, along with that from the rule of mixtures, is also shown. Both types of composites are significantly tougher than their constituents. In particular, the brick-and-mortar composites display K_c fracture toughnesses more than an order of magnitude larger than their principal constituent phase Al_2O_3. [The circles correspond to grafted (strong) interfaces and the squares to nongrafted (weaker) interfaces.] The error bars represent ±SD. (**B**) Specific strength and toughness (i.e., properties normalized by density) for a wide range of materials systems (*43*), showing that our hierarchical Al_2O_3/PMMA composites, some containing ~80 vol. % alumina ceramic, have strength/toughness properties comparable with that of metallic aluminum alloys.

of most monolithic structural ceramics with engineered grain boundaries, i.e., coarse-grained Al_2O_3, Si_3N_4, and SiC (*35*–*42*). However, the contribution from bridging alone does not explain why the observed toughness of the best brick-and-mortar 80% alumina structure (J_c ~ 8000 J/m^2) is more than 300 times higher in terms of energy than the toughness of its main constituent, Al_2O_3 (J_c ~ 26 J/m^2). We believe that of the various hybrid materials that we have fabricated, this structure best mimics nacre. Freeze casting followed by pressing and a second sintering stage results in a microstructure with high ceramic contents characterized by the submicrometer lubricating polymer interlayers between ceramic "bricks" (deformation and micrometer-scale tearing in these interlayers can be seen in Fig. 4A); combined with the roughness of the ceramic interfaces and the presence of stiff ceramic bridges between grains with micrometer and submicrometer dimensions (Fig. 1, C and D), this method promotes controlled sliding and "sliding interference" (Fig. 4) between the rough ceramic interlayers, thereby enhancing the toughness through extremely efficient energy dissipation. The result is synthetic materials that, like nacre and bone, are far tougher than what could be expected from the simple mixture of their constituents (Fig. 5A).

Concluding remarks and future challenges. A better appreciation of the unique mechanical properties of these freeze-cast composites can be gained by comparing them to other materials. By combining two relatively ordinary phases, i.e., a hard yet brittle ceramic with a relatively soft (in comparison) polymer, we have synthesized primarily (ceramic) alumina hybrid structures with specific strength and toughness properties that match those of engineering (metallic) aluminum alloys (Fig. 5B) and moreover display a higher stiffness. This has been made possible through the development of hierarchical architectures that combine toughening mechanisms acting at multiple scales, from submicrometer dimensions (i.e., the ceramic bridges between lamellae or bricks or the inelastic polymer deformation) and higher. These results highlight the tremendous potential of the biomimetic approach and suggest promising strategies for structural optimization. In particular, a key attribute of nacre has been extremely difficult to replicate: The structure consists of 95 vol. % ceramic with very little of the organic soft phase, which is distributed as a thin (2 to 3 nm) protein film that acts like a lubricant. At present, our materials contain too much of the soft phase, and our ceramic layer thicknesses are still somewhat coarse in comparison to nacre; indeed, a reduction in the polymer content and refinement of the ceramic layers should improve strength and provide additional nanoscale toughening mechanisms similar to those acting in natural materials. In this regard, our current studies are focused on the development of these hybrid structures with much higher inorganic content, the manipulation of the properties of the soft lubricating phase, and extending this concept to other material combinations, principally metal-infiltrated ceramics.

References and Notes

1. G. Mayer, *Science* **310**, 1144 (2005).
2. M. A. Meyers, P. Y. Chen, A. Y. M. Lin, Y. Seki, *Prog. Mater. Sci.* **53**, 1 (2008).
3. C. Ortiz, M. C. Boyce, *Science* **319**, 1053 (2008).
4. J. Aizenberg *et al*., *Science* **309**, 275 (2005).
5. F. Barthelat, H. D. Espinosa, *Exp. Mech.* **47**, 311 (2007).
6. R. K. Nalla, J. H. Kinney, R. O. Ritchie, *Biomaterials* **24**, 3955 (2003).
7. R. K. Nalla, J. J. Kruzic, J. H. Kinney, R. O. Ritchie, *Biomaterials* **26**, 217 (2005).
8. R. O. Ritchie, *Mater. Sci. Eng. A* **103**, 15 (1988).
9. R. Z. Wang, Z. Suo, A. G. Evans, N. Yao, I. A. Aksay, *J. Mater. Res.* **16**, 2485 (2001).
10. A. G. Evans *et al*., *J. Mater. Res.* **16**, 2475 (2001).
11. X. D. Li, W. C. Chang, Y. J. Chao, R. Z. Wang, M. Chang, *Nano Lett.* **4**, 613 (2004).
12. B. L. Smith *et al*., *Nature* **399**, 761 (1999).
13. F. Song, A. K. Soh, Y. L. Bai, *Biomaterials* **24**, 3623 (2003).
14. H. M. Chan, *Annu. Rev. Mater. Sci.* **27**, 249 (1997).
15. J. S. Moya, *Adv. Mater.* **7**, 185 (1995).
16. A. Sellinger *et al*., *Nature* **394**, 256 (1998).
17. Z. Tang, N. A. Kotov, S. Magonov, B. Ozturk, *Nat. Mater.* **2**, 413 (2003).
18. L. J. Bonderer, A. R. Studart, L. J. Gauckler, *Science* **319**, 1069 (2008).
19. P. Podsiadlo *et al*., *Science* **318**, 80 (2007).
20. S. Deville, E. Saiz, R. K. Nalla, A. P. Tomsia, *Science* **311**, 515 (2006).
21. S. Deville, E. Saiz, A. P. Tomsia, *Acta Mater.* **55**, 1965 (2007).
22. T. Fukasawa, M. Ando, T. Ohji, S. Kanzaki, *J. Am. Ceram. Soc.* **84**, 230 (2001).
23. T. Fukasawa, Z. Y. Deng, M. Ando, T. Ohji, Y. Goto, *J. Mater. Sci.* **36**, 2523 (2001).
24. K. Araki, J. W. Halloran, *J. Am. Ceram. Soc.* **87**, 1859 (2004).
25. K. J. Koester, J. W. Ager, R. O. Ritchie, *Nat. Mater.* **7**, 672 (2008).
26. A. Tasdemirci, I. W. Hall, B. A. Gama, M. Guiden, *J. Compos. Mater.* **38**, 995 (2004).
27. D. R. Johnson, X. F. Chen, B. F. Oliver, R. D. Noebe, J. D. Whittenberger, *Intermetallics* **3**, 99 (1995).
28. R. M. Jones, *Mechanics of Composite Materials* (Taylor & Francis, Philadelphia, PA, ed. 2, 1999).
29. Supporting online material on *Science* Online.
30. J. K. Shang, R. O. Ritchie, *Metallurg. Trans. A* **20**, 897 (1989).
31. Instead of crack extension being solely associated with the main crack tip growing forward, crack advance also can occur by microcracks (or other damage) initiated ahead of the main crack tip linking back to the tip.
32. J. Cook, C. C. Evans, J. E. Gordon, D. M. Marsh, *Proc. R. Soc. Lond. A Math. Phys. Sci.* **282**, 508 (1964).
33. L. S. Sigl, P. A. Mataga, B. J. Dalgleish, R. M. McMeeking, A. G. Evans, *Acta Metall.* **36**, 945 (1988).
34. A. Y. M. Lin, P. Y. Chen, M. A. Meyers, *Acta Biomater.* **4**, 131 (2008).
35. P. F. Becher *et al*., *J. Am. Ceram. Soc.* **81**, 2821 (1998).
36. J. J. Cao, W. J. MoberlyChan, L. C. DeJonghe, C. J. Gilbert, R. O. Ritchie. *J. Am. Ceram. Soc.* **79**, 461 (1996).
37. J. J. Kruzic, R. M. Cannon, R. O. Ritchie, *J. Am. Ceram. Soc.* **87**, 93 (2004).
38. J. J. Kruzic, R. M. Cannon, R. O. Ritchie, *J. Am. Ceram. Soc.* **88**, 2236 (2005).
39. F. F. Lange, *J. Am. Ceram. Soc.* **56**, 518 (1973).
40. Y. W. Mai, B. R. Lawn, *J. Am. Ceram. Soc.* **70**, 289 (1987).
41. N. P. Padture, B. R. Lawn, *J. Am. Ceram. Soc.* **77**, 2518 (1994).
42. P. L. Swanson, C. J. Fairbanks, B. R. Lawn, Y. W. Mai, B. J. Hockey, *J. Am. Ceram. Soc.* **70**, 279 (1987).
43. U. G. K. Wegst, M. F. Ashby, *Philos. Mag.* **84**, 2167 (2004).

44. This work was supported by the Director, Office of Science, Office of Basic Energy Sciences, Division of Materials Sciences and Engineering, of the U.S. Department of Energy under Contract No. DE-AC02-05CH11231

Supporting Online Material

www.sciencemag.org/cgi/content/full/322/5907/1516/DC1
Materials and Methods
Figs. S1 and S2
References

19 August 2008; accepted 21 October 2008
10.1126/science.1164865

Metallic and Insulating Phases of Repulsively Interacting Fermions in a 3D Optical Lattice

U. Schneider,[1] L. Hackermüller,[1] S. Will,[1] Th. Best,[1] I. Bloch,[1,2]* T. A. Costi,[3] R. W. Helmes,[4] D. Rasch,[4] A. Rosch[4]

The fermionic Hubbard model plays a fundamental role in the description of strongly correlated materials. We have realized this Hamiltonian in a repulsively interacting spin mixture of ultracold ^{40}K atoms in a three-dimensional (3D) optical lattice. Using in situ imaging and independent control of external confinement and lattice depth, we were able to directly measure the compressibility of the quantum gas in the trap. Together with a comparison to ab initio dynamical mean field theory calculations, we show how the system evolves for increasing confinement from a compressible dilute metal over a strongly interacting Fermi liquid into a band-insulating state. For strong interactions, we find evidence for an emergent incompressible Mott insulating phase. This demonstrates the potential to model interacting condensed-matter systems using ultracold fermionic atoms.

Interacting fermions in periodic potentials lie at the heart of condensed-matter physics, presenting some of the most challenging problems to quantum many-body theory. A prominent example is high-temperature superconductivity in cuprate compounds (*1*). An essential part of the physics in these systems is described by the fermionic Hubbard Hamiltonian (*2*), which models interacting electrons in a periodic potential (*1*, *3*). In a real solid, however, the effects of interest are typically complicated by, for example, multiple bands, impurities, and the long-range nature of Coulomb interactions, which becomes especially relevant close to a metal-to-insulator transition.